



High-Efficient and Broadband Acoustic Insulation in a Ventilated Channel With Acoustic Metamaterials

Zihao Su[†], Yifan Zhu^{*†}, Siyuan Gao, Hao Luo and Hui Zhang^{*}

Jiangsu Key Laboratory for Design and Manufacture of Micro-Nano Biomedical Instruments, School of Mechanical Engineering, Southeast University, Nanjing, China

OPEN ACCESS

Edited by:

Morvan Ouisse,
École Nationale Supérieure de
Mécanique et des Microtechniques,
France

Reviewed by:

Federico Bosia,
Politecnico di Torino, Italy
Abdelkrim Khelif,
UMR6174 Institut Franche Comté
Électronique Mécanique Thermique et
Optique Sciences et Technologies
(FEMTO-ST), France

*Correspondence:

Yifan Zhu
yifanzhu@seu.edu.cn
Hui Zhang
seuzhanghui@seu.edu.cn

[†]These authors have contributed
equally to this work

Specialty section:

This article was submitted to
Vibration Systems,
a section of the journal
Frontiers in Mechanical Engineering

Received: 19 January 2022

Accepted: 11 April 2022

Published: 18 May 2022

Citation:

Su Z, Zhu Y, Gao S, Luo H and
Zhang H (2022) High-Efficient and
Broadband Acoustic Insulation in a
Ventilated Channel With
Acoustic Metamaterials.
Front. Mech. Eng 8:857788.
doi: 10.3389/fmech.2022.857788

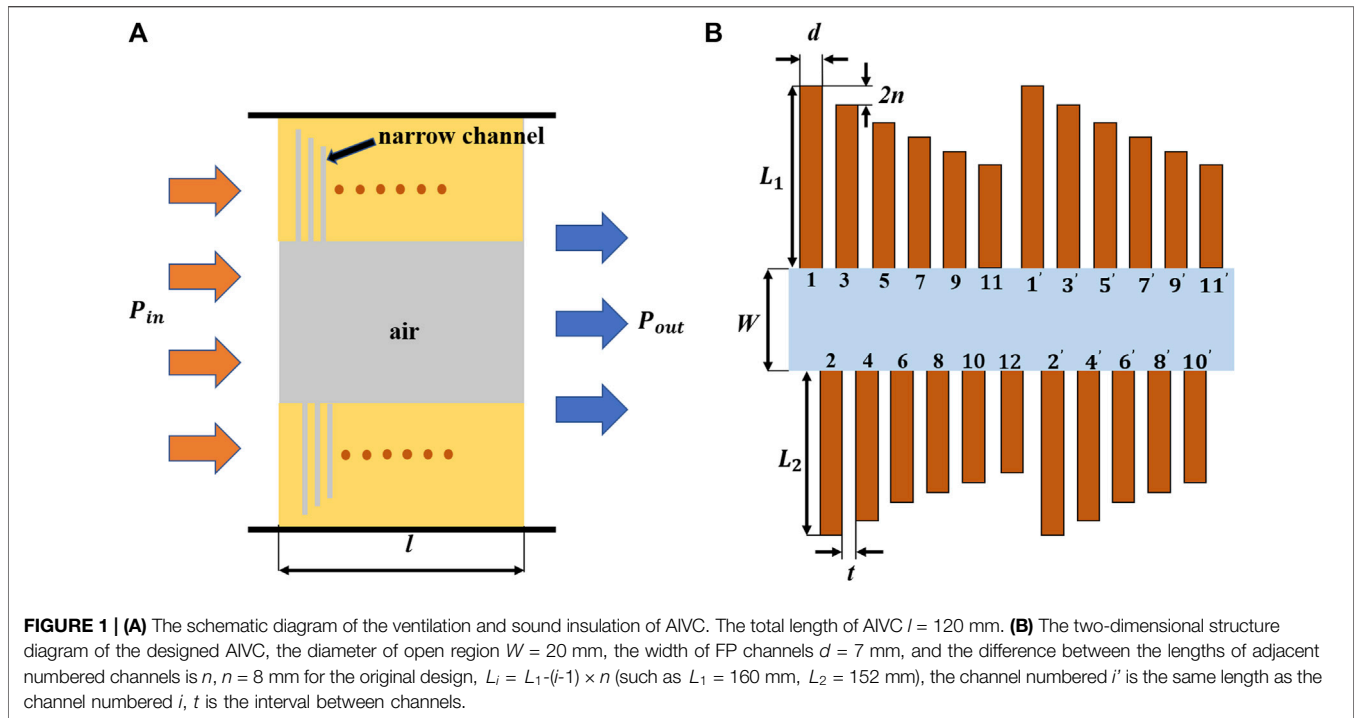
Acoustic insulation in ventilated structures is an important problem in acoustic engineering with many potential practical applications, such as the noise control for ventilating ducts of buildings, vehicles, or air conditioners. Acoustic metamaterial is a good candidate for the design of acoustic insulation for ventilated channel (AIVC) because the structural design with hard boundary has longer lifetime than conventional sound-absorbing cotton. In this paper, an AIVC with an open region and narrow channels of different lengths is proposed. We numerically and experimentally demonstrate its acoustic insulation larger than 20 dB ($T < 0.01$) within approximately 500–1,200 Hz with a subwavelength channel length of $\lambda/6$. The parameter dependence and air flow effect are numerically studied. Our findings show an alternative design of AIVC that may have applications in noise control and architectural acoustics.

Keywords: acoustic metamaterial, acoustic insulation, ventilated channel, broadband, acoustics

INTRODUCTION

In acoustic engineering, it is a key scientific problem to achieve low frequency and broadband noise control by sound absorptions or sound insulations. In the past decades, acoustic metamaterials (Cummer et al., 2016; Ma and Sheng, 2016) and acoustic metasurfaces (Assouar et al., 2018) have become the most promising candidates for noise control engineering and advanced acoustic material design and manufacture, due to their physical characteristics, shape controllability and small volume/size. Acoustic metamaterial/metamaterial-based absorbers have been designed for ultra-broadband working bandwidth (Jiang et al., 2014; Yang et al., 2017; Zhu et al., 2019; Huang et al., 2020; Kumar and Lee, 2020; Zhu et al., 2021), ultra-light mass (Yang et al., 2008; Yang et al., 2010; Yao et al., 2010; Mei et al., 2012; Fan et al., 2015; Huang et al., 2016; Gao et al., 2017; Gao et al., 2018; Li et al., 2020; Zhang et al., 2020) and ultrathin sample thickness (Li and Assouar, 2016; Donda et al., 2019; Donda et al., 2021), which benefit the development of conceptual acoustic device called acoustic meta-absorber.

Acoustic absorption (Li et al., 2018; Wu et al., 2018) and insulation (Yang et al., 2018) by acoustic metamaterials in ventilated structures is another important problem in acoustic engineering with many potential practical applications, such as the noise control for the ventilating ducts of buildings, vehicles, or air conditioners. In previous works, acoustic insulation ventilated channels (AIVC) have been designed with the help of acoustic metamaterials (Zhang et al., 2017; Lee et al., 2019; Sun et al., 2020; Dong et al., 2021; Shen et al., 2021). Considering the tradeoff between sample size and working efficiency, previous balanced designs always have an average absorption within approximately 0.85–0.95 (Jiang et al., 2014; Yang et al., 2017; Zhang et al., 2017; Lee et al., 2019; Zhu et al., 2019; Huang et al., 2020; Dong et al., 2021; Shen et al., 2021; Zhu et al., 2021). However, high-efficient sound insulation is very important and significant for acoustic engineering applications. A high sound insulation index (close to 1) is highly desirable for many practical cases when the intensity of noise source is very large, such as the noises from construction sites or large-scale vehicles.



In this paper, an AIVC with an open region and narrow channels of different lengths is proposed. We numerically and experimentally demonstrate its acoustic insulation larger than 20 dB (meaning sound intensity transmission $T < 0.01$) within approximately 500–1,200 Hz with a subwavelength channel length of $\lambda/6$. This high transmission loss is very important in many practical sound insulation occasions. We have designed the channel lengths with different distributions, such as the linear one and the optimized one. More parameter dependence of the AIVC is studied, such as the different open region widths from 15 to 40 mm, and different narrow channel widths from 6 to 9 mm. Our findings show an alternative design for perfect sound insulation with a high sound reduction index, that may have applications in environmental acoustics and architectural acoustics.

DESIGN METHOD

The method reported in this paper enables the design of open-type acoustic metamaterials consisting of narrow Fabry-Pérot (FP) channels (Jiang et al., 2014; Yang et al., 2017; Xiao et al., 2021) with open region that provide high sound attenuation and adequate ventilation performance. Inspired by previous work (Deng et al., 2017; Ghaffarivardavagh et al., 2019; Shi et al., 2021), the FP channels are used as a side branch, which greatly improve the sound insulation performance of the structure, while retaining the opening part to ensure its ventilation performance. The schematic diagram of the designed AIVC is shown in Figure 1. The parameters are marked in the figure. For an original design, the total length of AIVC is $l = 120$ mm. The diameter of open region $W = 20$ mm, the width of FP channels $d = 7$ mm, the difference between the lengths of adjacent numbered channels is n , $n = 8$ mm for the original design. t is the interval between

channels and the sum of d and t is a constant value. As shown in Figure 1A, the sound wave passes through the open region with the periodically arranged side branches, the walls of the side branches can be assumed to be rigid, and the medium in the channels is air. Distributing the narrow tubes on both sides not only saves space, but also enhances coupling and improves sound insulation performance. The incident acoustic wave will be coupled with different FP channels and dissipated inside. In Figure 1B, the length of the channels varies linearly (relative to the number i). The number i annotated in Figure 1B from 1 to 12 denotes the cells with first-order peak frequency from lower to higher. It is noted that Figure 1B shows a periodic arrangement (1–11 and 1'–11') which is an original design but not necessary in our work. We will show other non-periodic designs in the following.

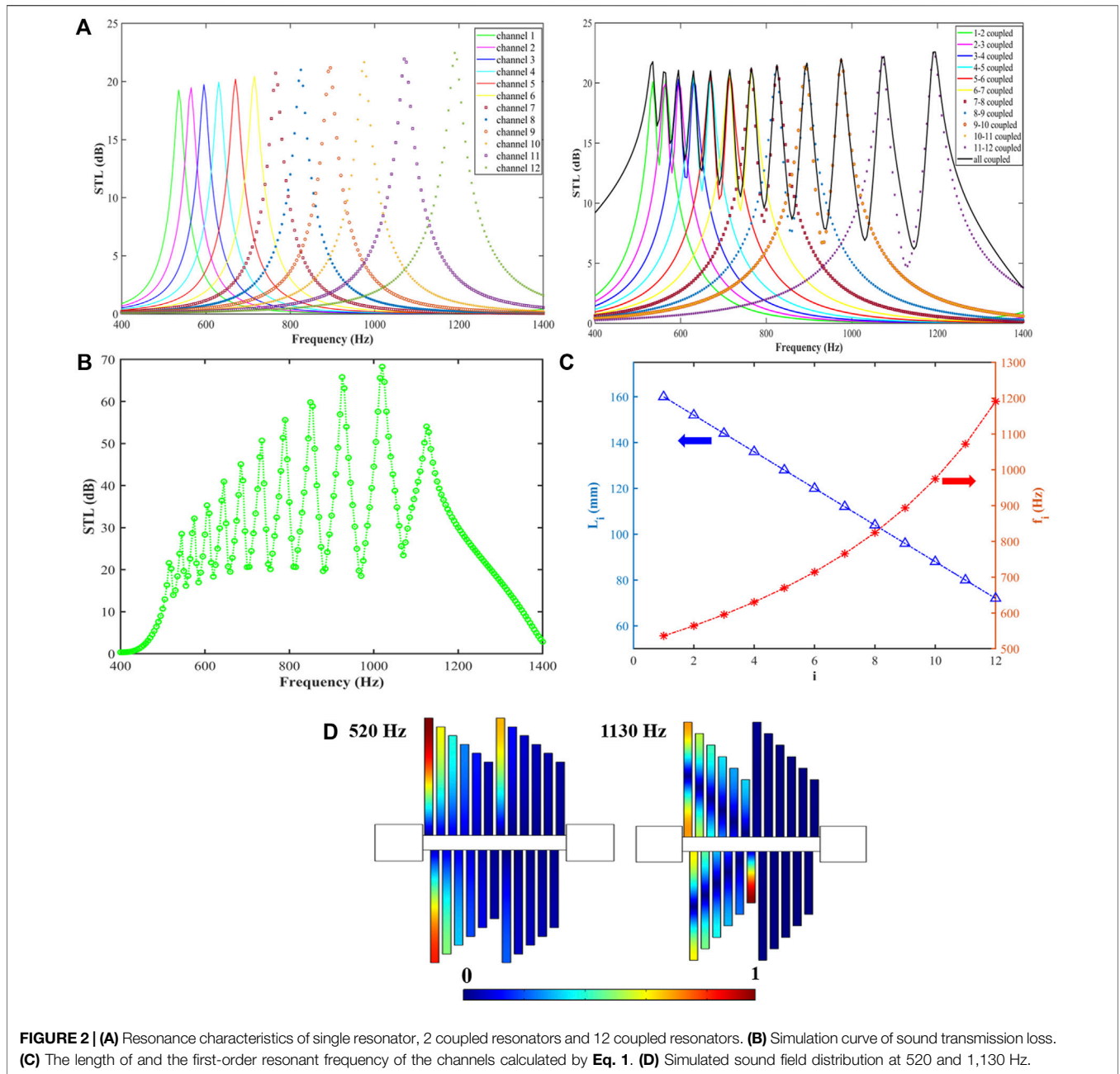
The first-order resonance frequency is determined by the length of the FP resonance channel, and their relationship can be described as

$$f_i = c_0 / 4L_i \tag{1}$$

where c_0 is the sound speed in the air, and L_i is the length of FP channel, f_i is the resonant frequency corresponding to the channel length. Thermal viscous effects in the channels need to be considered, especially at resonant frequencies. The attenuation coefficient α in the channel is

$$\alpha \approx \frac{2}{dc_0} \sqrt{\frac{\eta\omega}{2\rho_0}} \tag{2}$$

where ω is the angular frequency, η and ρ_0 are the viscosity coefficient and mass density of air, respectively. Due to the existence of resonance, the thermal viscous loss in the channel

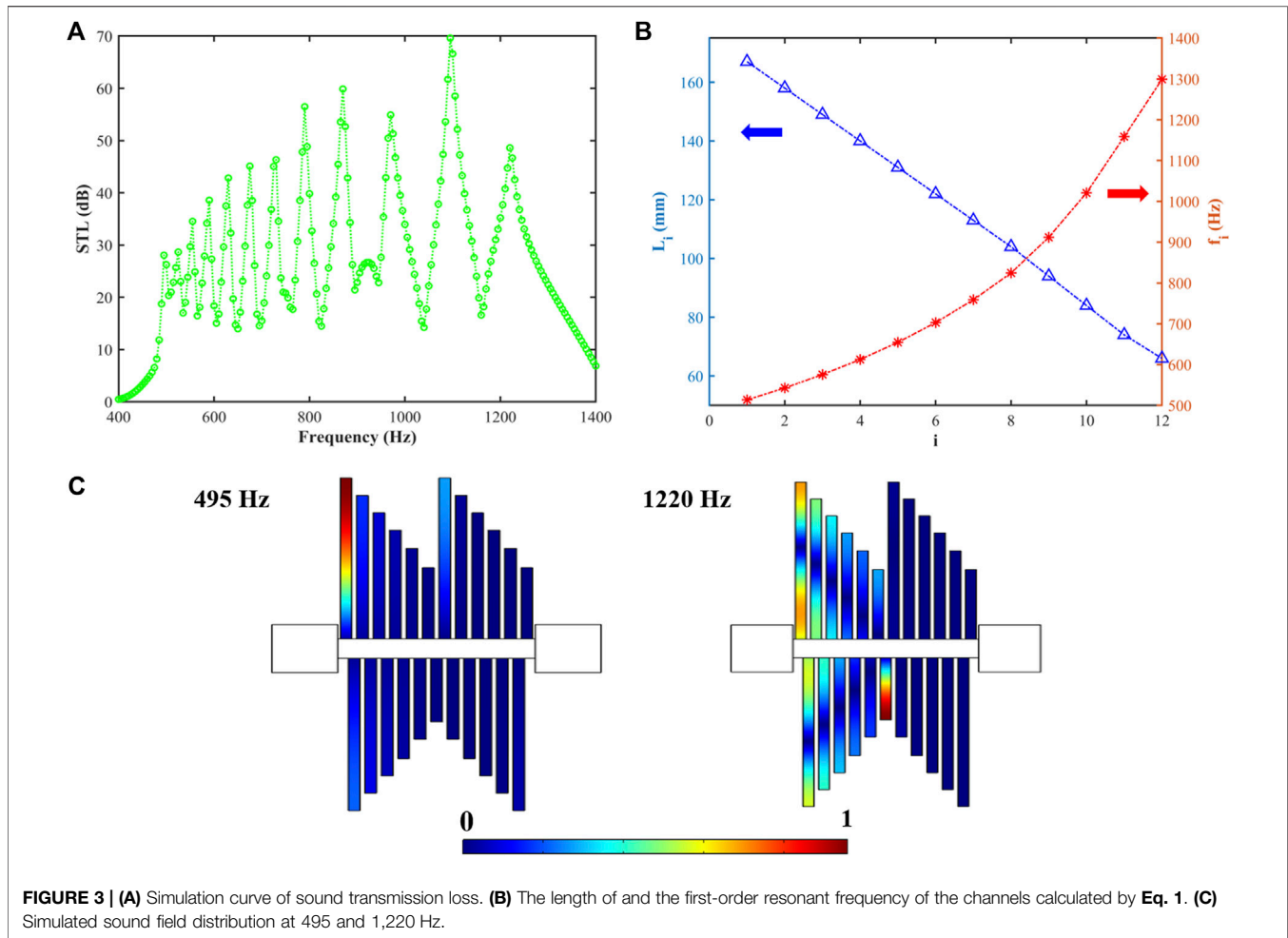


will be greatly enhanced, and the coupling of the two effects enhances the sound insulation capability of the structure.

NUMERICAL SIMULATIONS

To verify the sound insulation effect of the structure, numerical simulations have been performed by the commercial finite element software COMSOL. The Viscous effect has been considered in the simulations in the Thermoviscous Acoustics Module and the results are shown in Figure 2. To understand completely the mechanism of the

broadband acoustic insulation, Figure 2A shows the sound transmission loss (STL) curves for a single resonator, two coupled resonators with slightly different lengths, and 12 coupled resonators, respectively. The results suggest that the coupling of the unit cells leads to the connection of STL spectrum. From Figure 2B, an ultra-broadband sound insulation of more than 20 dB can be observed, approximately from 520 to 1,280 Hz, over an octave. The sound transmission loss band consists of 12 peaks, which correspond to 12 FP resonant channels of different lengths. The lengths of the channels and their corresponding resonant frequencies calculated by Eq. 1 are shown in Figure 2C.



By comparing **Figures 2B,C**, it can be clearly seen that the resonant frequency at the peak of the sound transmission loss band is observed not exactly at the resonant frequency of the single resonant channel, owing to the coupling effects of the whole structure. To further explain this phenomenon, **Figure 2D** shows the simulated acoustic pressure amplitude field at 520 and 1,130 Hz, respectively. These two frequencies correspond to the first and 12th (last) peaks, respectively. Different from the traditional FP resonance channels, the staggered arrangement makes the FP resonance channels no longer act individually, but the adjacent numbered channels act simultaneously, thus resulting in the shift of the peak frequency to low frequency. As can be seen in **Figure 2D**, at 520 Hz, the dominant channels are 1, 2 and 1', not just 1 and 1'. After passing through the 1' channel, there is no high sound pressure distribution in the rear channels, which proves the effectiveness of the sound insulation of the structure. The same effect can also be observed in the sound field distribution diagram at 1,130 Hz. A higher sound pressure appears in the 12th channel, which blocks the sound from propagating backwards, so a lower sound pressure distribution appears in the rear channels.

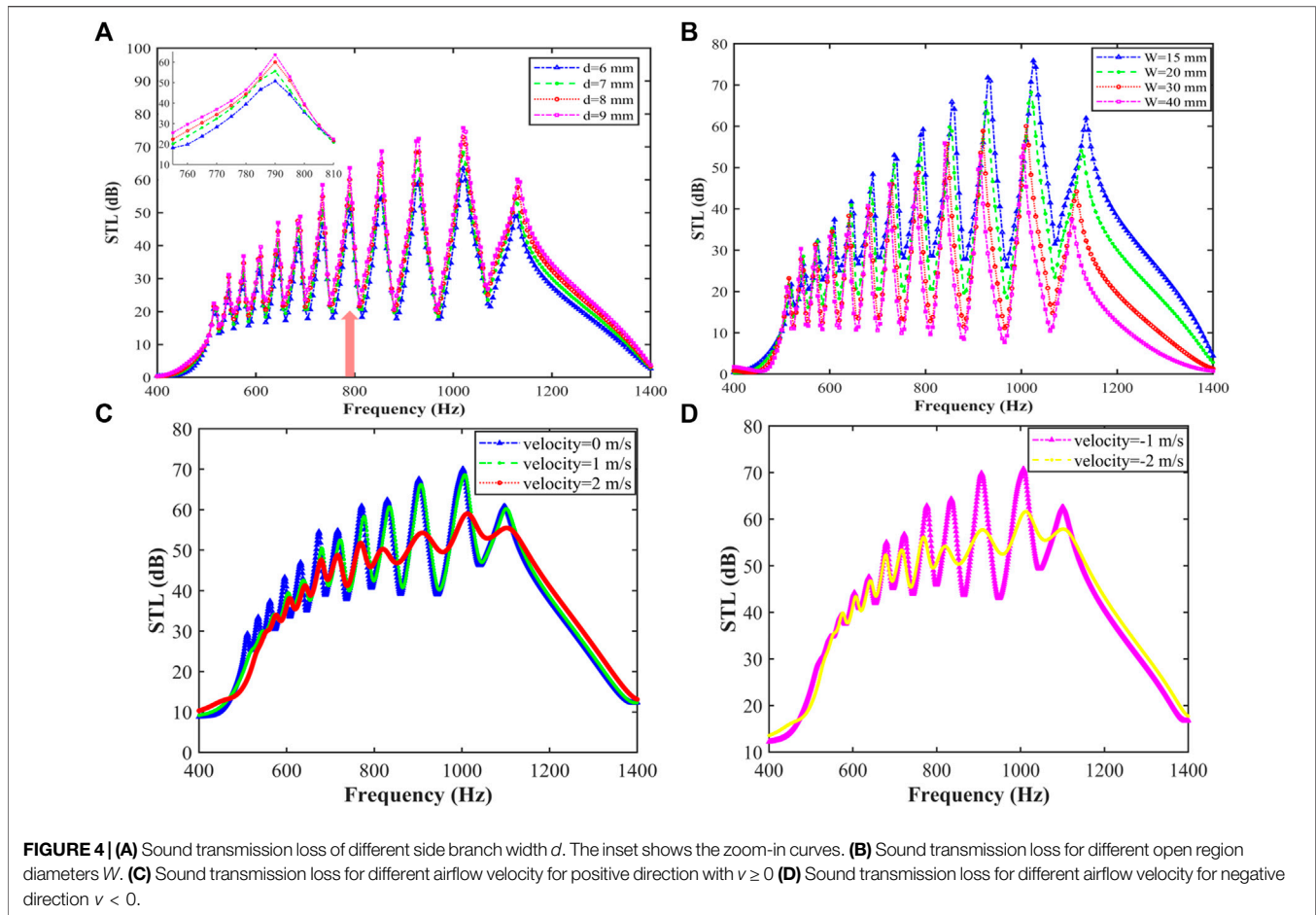
To further improve the performance of the structure, the channel length and distribution were changed from linear to nonlinear, and the symmetry is changed for the bottom narrow

channels, as shown in **Figure 3**. The sound insulation performance has dropped slightly, for which some valley values are below 20 dB. Interestingly, the STL bandwidth covers the frequency range from 490 to 1,330 Hz. Compared to the design in **Figure 2**, the bandwidth for sound insulation is increased, due to the fact that the resonant absorption frequencies are optimized, and the change of the symmetry for bottom narrow channels can alter the coupling effects between adjacent unit cells.

PARAMETER DEPENDENCES AND AIR FLOW EFFECT

We further investigated the dependence of the sound insulation effect on the diameter of the open region and the FP resonant channel width. In practice, there should be reasonable structural dimensions while maintaining the performance of sound insulation.

Figure 4A shows the sound transmission loss of AIVC as a function of frequency with different d values from 6 to 9 mm. The simulation results prove that the broadband characteristics of AIVC are hardly affected by the variation of channel width, and the apparent difference only appears at the peaks as shown in the



inset of **Figure 4A**. The larger d value has higher sound insulation because of the better coupling at the opening of the narrow channel. The changing the diameter of the FP resonant channel will only affect the performance at the peak frequency, and has little effect on the bandwidth and performance at other frequencies.

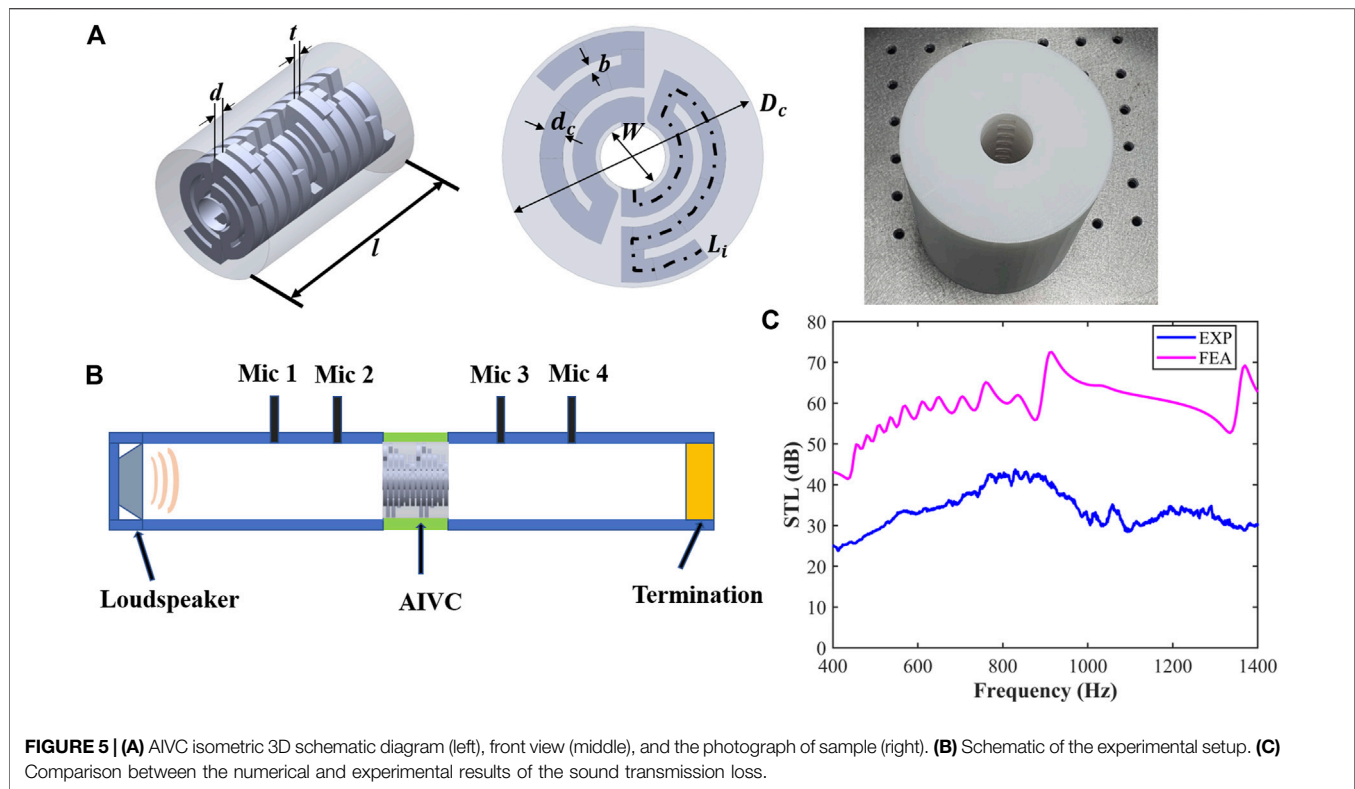
Figure 4B shows the sound transmission loss curves with different open region widths. The four curves correspond to four different open region widths of 15 mm, 20 mm, 30 mm and 40 mm, respectively. It can be observed that as the open region width is significantly reduced, the acoustic transmission is effectively suppressed, and at the same time, an improvement in performance over the entire frequency band is achieved. This result indicates that there is a tradeoff between the ventilated area and sound insulation efficiency.

We also study the influence of air flow effects in the ventilated channel for sound insulation. Aeroacoustics Module of the COMSOL software is used to study the air flow effect in AIVC. The corresponding simulated results are shown in **Figures 4C,D** with positive and negative airflows, respectively. The results show that the airflow effect has an obvious influence on sound insulation. When the velocity of the medium v (background mean flow velocity) is 0 m/s, the STL curve is in high agreement with **Figure 2B**. As the medium velocity increases, the peaks at low frequencies and the sound insulation decreases slightly.

EXPERIMENT DEMONSTRATION OF A 3D DESIGN

In order to experimentally verify the performance of AIVC in terms of sound insulation, an experimental sample is fabricated via a 3D printing technique in **Figure 5**. As shown in **Figure 5A**, the sample is designed as a ventilation structure with folded channels and a circular cross section (diameter = 10 cm) whose size agrees with standard acoustic impedance tube. We use folded channels in 3D case to replace straight channels in 2D case for the convenience of sample fabrications and experimental demonstration. The centre portion of the designed structure is a completely open region which yields a high degree of airflow. To be consistent with the 3D simulation, we fabricated the sample with PLA as the 3D printing material, which can be regarded as a hard boundary. The arrangement of the side branches is the same as in **Figure 2**, and the structure size is slightly changed, where $d = 8.75$ mm, $t = 3.75$ mm, $l = 150$ mm, $D_c = 100$ mm, $W = 25$ mm, $d_c = 8.75$ mm, $b = 3.75$ mm, $L_1 = 200$ mm, $L_i = L_1 - (i-1) \times n$, $n = 10$ mm.

The experimental setup is shown in **Figure 5B**. The four microphones method is adopted to measure the transmission loss of the AIVC. A loudspeaker is placed at one end of the impedance tube. Termination is set as sound absorption termination for



sound insulation measurement. The sample is placed in the middle.

The experimental results are shown in **Figure 5C**. The numerical (experimental) STL for sound insulation is large than 40 dB (25 dB) within 400–1,400 Hz, and the averaged STL in this band is approximately 55 dB (35 dB). The sound insulation effect for 3D design is better than 2D ones. This is probably because the 3D one makes full use of the space, and the coupled effect between unit cells for 3D case is better. The difference between numerical and experimental STL is approximately 20 dB. This value difference seems to be large with exponential units (dB), but the STL of both exceeds 20 dB, which means that more than 99% of the sound energy is blocked. So the experimental one has a high-efficient insulation as well as the numerical one. The averaged error between numerical and experimental ones is less than 0.06, which may be due to the imperfect of sample fabrications and slight leakage of sound.

CONCLUSION

In summary, we have theoretically demonstrated a broadband low-frequency soundproof ventilation channel with a structural thickness of only 120 mm (about $\lambda/6$), which can effectively block more than 99% of the incident sound energy in the range of about 500–1,200 Hz and have experimentally verified our proposal. The ventilation channel consists of a central open region and 12 kinds of side branches consisting of different length narrow channels. By adjusting the distribution of side branch channels, high sound

insulation performance is achieved, and the simulation and experimental results successfully verified our theory. At the same time, we also considered the influence of the width of the opening region, the width of the side branch channel and air flow effect (including flow speed and direction) on the sound insulation performance. Our work proposes a design concept of low-frequency broadband, low-thickness and high-efficient ventilation channel structure, which can help noise control and could be widely used in architectural acoustics through the reasonable design of dimensions.

DATA AVAILABILITY STATEMENT

The raw data supporting the conclusions of this article will be made available by the authors, without undue reservation.

AUTHOR CONTRIBUTIONS

ZS, SG, HL, and YZ do the simulations. ZS, YZ, and HZ write the manuscript. HZ guide the research.

FUNDING

The authors acknowledge the financial support provided by the National Natural Science Foundation of China (No. 11874110).

REFERENCES

- Assouar, B., Liang, B., Wu, Y., Li, Y., Cheng, J.-C., and Jing, Y. (2018). Acoustic Metasurfaces. *Nat. Rev. Mater.* 3 (12), 460–472. doi:10.1038/s41578-018-0061-4
- Cummer, S. A., Christensen, J., and Alù, A. (2016). Controlling Sound with Acoustic Metamaterials. *Nat. Rev. Mater.* 1 (3), 16001. ARTN. doi:10.1038/natrevmats.2016.1
- Deng, Y.-Q., Qi, D.-X., Tuo, M.-J., Liu, L.-Z., Zhang, R.-L., and Peng, R.-W. (2017). Multimode Acoustic Transparency and Slow Sound Effects in Hybrid Subwavelength Resonators. *Appl. Phys. Express* 10(3), 037302 Art. doi:10.7567/Apex.10.037302
- Donda, K., Zhu, Y. F., Fan, S. W., Cao, L. Y., Li, Y., and Assouar, B. (2019). Extreme Low-Frequency Ultrathin Acoustic Absorbing Metasurface. *Appl. Phys. Lett.* 115 (17), 173506. Art. doi:10.1063/1.5122704
- Donda, K., Zhu, Y. F., Merkel, A., Fan, S. W., Cao, L. Y., Wan, S., et al. (2021). Ultrathin Acoustic Absorbing Metasurface Based on Deep Learning Approach. *Smart Mater. Structures* 30 (8), 085003. ARTN. doi:10.1088/1361-665X/ac0675
- Dong, R., Mao, D., Wang, X., and Li, Y. (2021). Ultrabroadband Acoustic Ventilation Barriers via Hybrid-Functional Metasurfaces. *Phys. Rev. Appl.* 15 (2), 24044. doi:10.1103/PhysRevApplied.15.024044
- Fan, L., Chen, Z., Zhang, S. Y., Ding, J., Li, X. J., and Zhang, H. (2015). An Acoustic Metamaterial Composed of Multi-Layer Membrane-Coated Perforated Plates for Low-Frequency Sound Insulation. *Appl. Phys. Lett.* 106 (15), 151908. Art. doi:10.1063/1.4918374
- Gao, N., Hou, H., and Wu, J. H. (2018). A Composite and Deformable Honeycomb Acoustic Metamaterial. *Int. J. Mod. Phys. B* 32 (20), 2041. doi:10.1142/s0217979218502041
- Gao, N. S., Wu, J. H., Hou, H., and Yu, L. (2017). Excellent Low-Frequency Sound Absorption of Radial Membrane Acoustic Metamaterial. *Int. J. Mod. Phys. B* 31 (3), 1750011. Art. doi:10.1142/S0217979217500114
- Ghaffarivardavagh, R., Nikolajczyk, J., Anderson, S., and Zhang, X. (2019). Ultra-Open Acoustic Metamaterial Silencer Based on Fano-Like Interference. *Phys. Rev. B* 99 (2), 024302. ARTN. doi:10.1103/PhysRevB.99.024302
- Huang, S. B., Zhou, Z. L., Li, D. T., Liu, T., Wang, X., Zhu, J., et al. (2020). Compact Broadband Acoustic Sink with Coherently Coupled Weak Resonances. *Sci. Bull.* 65 (5), 373–379. doi:10.1016/j.scib.2019.11.008
- Huang, T. Y., Shen, C., and Jing, Y. (2016). Membrane- and Plate-Type Acoustic Metamaterials. *J. Acoust. Soc. Am.* 139 (6), 3240. doi:10.1121/1.4950751
- Jiang, X., Liang, B., Li, R. Q., Zou, X. Y., Yin, L. L., and Cheng, J. C. (2014). Ultra-Broadband Absorption by Acoustic Metamaterials. *Appl. Phys. Lett.* 105 (24), 243505. Art. doi:10.1063/1.4904887
- Kumar, S., and Lee, H. P. (2020). Labyrinthine Acoustic Metastructures Enabling Broadband Sound Absorption and Ventilation. *Appl. Phys. Lett.* 116 (13), 134103. Art. doi:10.1063/5.0004520
- Lee, T., Nomura, T., Dede, E. M., and Iizuka, H. (2019). Ultrasparse Acoustic Absorbers Enabling Fluid Flow and Visible-Light Controls. *Phys. Rev. Appl.* 11 (2), 024022. ARTN. doi:10.1103/PhysRevApplied.11.024022
- Li, L. J., Zheng, B., Zhong, L. M., Yang, J., Liang, B., and Cheng, J. C. (2018). Broadband Compact Acoustic Absorber with High-Efficiency Ventilation Performance. *Appl. Phys. Lett.* 113 (10), 103501. Art. doi:10.1063/1.5038184
- Li, Y., and Assouar, B. M. (2016). Acoustic Metasurface-Based Perfect Absorber with Deep Subwavelength Thickness. *Appl. Phys. Lett.* 108 (6), 063502. Art. doi:10.1063/1.4941338
- Li, Y., Zhang, Y., and Xie, S. (2020). A Lightweight Multilayer Honeycomb Membrane-Type Acoustic Metamaterial. *Appl. Acoust.* 168. doi:10.1016/j.apacoust.2020.107427
- Ma, G. C., and Sheng, P. (2016). Acoustic Metamaterials: From Local Resonances to Broad Horizons. *Sci. Adv.* 2 (2), e1501595. ARTN. doi:10.1126/sciadv.1501595
- Mei, J., Ma, G. C., Yang, M., Yang, Z. Y., Wen, W. J., and Sheng, P. (2012). Dark Acoustic Metamaterials as Super Absorbers for Low-Frequency Sound. *Nat. Commun.* 3, 756. ARTN. doi:10.1038/ncomms1758
- Shen, L., Zhu, Y. F., Mao, F. L., Gao, S. Y., Su, Z. H., Luo, Z. T., et al. (2021). Broadband Low-Frequency Acoustic Metamaterial. *Phys. Rev. Appl.* 16 (6), 064057. ARTN. doi:10.1103/PhysRevApplied.16.064057
- Shi, J. J., Liu, C. K., Liu, X. Z., and Lai, Y. (2021). Ventilative Meta-Window with Broadband Low-Frequency Acoustic Insulation. *J. Appl. Phys.* 129 (9), 094901. Art. doi:10.1063/5.0042384
- Sun, M., Fang, X. S., Mao, D. X., Wang, X., and Li, Y. (2020). Broadband Acoustic Ventilation Barriers. *Phys. Rev. Appl.* 13 (4), 044028. ARTN. doi:10.1103/PhysRevApplied.13.044028
- Wu, X. X., Au-Yeung, K. Y., Li, X., Roberts, R. C., Tian, J. X., Hu, C. D., et al. (2018). High-Efficiency Ventilated Metamaterial Absorber at Low Frequency. *Appl. Phys. Lett.* 112 (10), 103505. Art. doi:10.1063/1.5025114
- Xiao, Z. Q., Gao, P. L., Wang, D. W., He, X., and Wu, L. Z. (2021). Ventilated Metamaterials for Broadband Sound Insulation and Tunable Transmission at Low Frequency. *Extreme Mech. Lett.* 46, 101348. ARTN. doi:10.1016/j.eml.2021.101348
- Yang, J., Lee, J. S., Lee, H. R., Kang, Y. J., and Kim, Y. Y. (2018). Slow-Wave Metamaterials for Broadband Sound Insulation and Efficient Reduction of Low-Frequency Sound Transmission. *Appl. Phys. Lett.* 112 (9), 091901. Art. doi:10.1063/1.5003455
- Yang, M., Chen, S. Y., Fuab, C. X., and Sheng, P. (2017). Optimal Sound-Absorbing Structures. *Mater. Horizons* 4 (4), 673–680. doi:10.1039/c7mh00129k
- Yang, Z., Dai, H. M., Chan, N. H., Ma, G. C., and Sheng, P. (2010). Acoustic Metamaterial Panels for Sound Attenuation in the 50–1000 Hz Regime. *Appl. Phys. Lett.* 96 (4), 9007. doi:10.1063/1.3299007
- Yang, Z., Mei, J., Yang, M., Chan, N. H., and Sheng, P. (2008). Membrane-Type Acoustic Metamaterial with Negative Dynamic Mass. *Phys. Rev. Lett.* 101 (20), 204301. ARTN. doi:10.1103/PhysRevLett.101.204301
- Yao, S. S., Zhou, X. M., and Hu, G. K. (2010). Investigation of the Negative-Mass Behaviors Occurring Below a Cut-Off Frequency. *New J. Phys.* 12, 103025. Art. doi:10.1088/1367-2630/12/10/103025
- Zhang, H., Chen, S. B., Liu, Z. Z., Song, Y. B., and Xiao, Y. (2020). Light-Weight Large-Scale Tunable Metamaterial Panel for Low-Frequency Sound Insulation. *Appl. Phys. Express* 13 (6), 067003. ARTN. doi:10.35848/1882-0786/ab916b
- Zhang, H. L., Zhu, Y. F., Liang, B., Yang, J., Yang, J., and Cheng, J. C. (2017). Omnidirectional Ventilated Acoustic Barrier. *Appl. Phys. Lett.* 111 (20), 203502. Art. doi:10.1063/1.4993891
- Zhu, Y. F., Donda, K., Fan, S. W., Cao, L. Y., and Assouar, B. (2019). Broadband Ultra-Thin Acoustic Metasurface Absorber with Coiled Structure. *Appl. Phys. Express* 12 (11), 114002. ARTN. doi:10.7567/1882-0786/ab494a
- Zhu, Y., Merkel, A., Donda, K., Fan, S., Cao, L., and Assouar, B. (2021). Nonlocal Acoustic Metasurface for Ultrabroadband Sound Absorption. *Phys. Rev. B* 103 (6), 64102. doi:10.1103/PhysRevB.103.064102

Conflict of Interest: The authors declare that the research was conducted in the absence of any commercial or financial relationships that could be construed as a potential conflict of interest.

Publisher's Note: All claims expressed in this article are solely those of the authors and do not necessarily represent those of their affiliated organizations, or those of the publisher, the editors and the reviewers. Any product that may be evaluated in this article, or claim that may be made by its manufacturer, is not guaranteed or endorsed by the publisher.

Copyright © 2022 Su, Zhu, Gao, Luo and Zhang. This is an open-access article distributed under the terms of the Creative Commons Attribution License (CC BY). The use, distribution or reproduction in other forums is permitted, provided the original author(s) and the copyright owner(s) are credited and that the original publication in this journal is cited, in accordance with accepted academic practice. No use, distribution or reproduction is permitted which does not comply with these terms.